Monthly Notices
of the
ROYAL ASTRONOMICAL SOCIETY

MNRAS **447,** 1911–1921 (2015) doi:10.1093/mnras/stu2482

Luminosity function and jet structure of Gamma-Ray Burst

A. Pescalli,[1,2]★ G. Ghirlanda,[2] O. S. Salafia,[1,2] G. Ghisellini,[2] F. Nappo[3,2] and R. Salvaterra[4]

[1]*Dipartimento di Fisica G. Occhialini, Università di Milano Bicocca, Piazza della Scienza 3, I-20126 Milano, Italy*
[2]*INAF – Osservatorio Astronomico di Brera, via E. Bianchi 46, I-23807 Merate, Italy*
[3]*Universita' degli Studi dellInsubria, via Valleggio 11, I-22100 Como, Italy*
[4]*INAF – IASF Milano, via E. Bassini 15, I-20133 Milano, Italy*

Accepted 2014 November 23. Received 2014 October 29; in original form 2014 September 1

ABSTRACT

The structure of gamma-ray burst (GRB) jets impacts on their prompt and afterglow emission properties. The jet of GRBs could be *uniform*, with constant energy per unit solid angle within the jet aperture, or it could be *structured*, namely with energy and velocity that depend on the angular distance from the axis of the jet. We try to get some insight about the still unknown structure of GRBs by studying their luminosity function. We show that low (10^{46-48} erg s^{-1}) and high (i.e. with $L \geq 10^{50}$ erg s^{-1}) luminosity GRBs can be described by a unique luminosity function, which is also consistent with current lower limits in the intermediate luminosity range (10^{48-50} erg s^{-1}). We derive analytical expressions for the luminosity function of GRBs in uniform and structured jet models and compare them with the data. Uniform jets can reproduce the entire luminosity function with reasonable values of the free parameters. A structured jet can also fit adequately the current data, provided that the energy within the jet is relatively strongly structured, i.e. $E \propto \theta^{-k}$ with $k \geq 4$. The classical $E \propto \theta^{-2}$ structured jet model is excluded by the current data.

Key words: radiation mechanisms: non-thermal – relativistic processes – gamma-ray burst: general.

1 INTRODUCTION

Jets are a common feature of high-energy astrophysical sources powered by accretion on to compact objects. Gamma-Ray Burst (GRB) jets are thought to be the most extreme in terms of typical power (10^{50-54} erg s^{-1}) and of Lorentz factor ($\Gamma \sim 10^2$–10^3). Long GRBs are thought to follow the gravitational collapse of massive stars which form a rotating black hole with a bipolar jet along its rotational axis. The large isotropic equivalent energy $E_{\rm iso}$ of the prompt emission can exceed a solar mass rest energy, unless the radiation is collimated (Tan, Matzner & McKee 2001). The observed steepening of the afterglow flux light curve a few days after the burst is interpreted as the direct evidence of the presence of collimation.

It has been typically assumed that GRBs have a *Uniform Jet* (UJ): the energy and ejecta velocity are constant, within the jet aperture, and zero outside the jet opening angle (i.e. sharp-edged jet). During the afterglow phase, when the emission is produced by the deceleration of the relativistic jet by the interstellar medium, a steepening of the observed afterglow flux is predicted when $\Gamma \sim 1/\theta_{\rm j}$ (Rhoads 1997; Sari, Piran & Halpern 1999). The measure of the time of this break ($t_{\rm break}$) has been used to infer the jet opening angle $\theta_{\rm j}$ which results distributed in the 1°–10° range (Frail et al. 2001; Bloom, Frail & Kulkarni 2003; Ghirlanda et al. 2007). Intriguingly, the true energetic of GRBs (i.e. accounting for their collimation) clusters around a typical value $E_\gamma = E_{\gamma,\rm iso}(1 - \cos\theta_{\rm j}) \approx 10^{51}$ erg with a dispersion of less than a decade (Frail et al. 2001), correlating with the peak energy of the prompt emission spectrum $E_{\rm peak}$ (Ghirlanda, Ghisellini & Lazzati 2004; Nava et al. 2006). Such typical value for the true energy of GRBs is also directly probed by late-time radio observations (Frail, Waxman & Kulkarni 2000; Frail et al. 2005; Shivvers & Berger 2011).

For small jet angles, the collimation corrected $E_\gamma \propto \theta_{\rm j}^2 E_{\gamma,\rm iso}$. The small dispersion of E_γ led to the idea that the jet is not uniform, but *structured*, where θ is the angular distance from the jet axis, and coincides with the viewing angle $\theta_{\rm v}$. This scenario assumes that what we believed to be the jet angle $\theta_{\rm j}$ is actually the viewing angle $\theta_{\rm v}$. This can lead to a unification scheme in which all bursts have a quasi-universal jet configuration with a standard energy reservoir, but they appear different only because are seen under different angles. If the dependence of the burst energetics on θ is $E_{\gamma,\rm iso} \propto \theta^{-2}$, one recovers the finding of Frail et al. (2001) of the clustering of E_γ. These GRBs with a universal structured jet (SJ) were first proposed by Lipunov, Postnov & Prokhorov (2001) and then studied by Rossi, Lazzati & Rees (2002) and Zhang & Meszaros (2002). Some structure to the jet power and velocity could be imprinted, within the collapsar model, by the interaction

★ E-mail: a.pescalli@campus.unimib.it

of the jet with the star (e.g. Lyutikov & Blandford 2002; Levinson & Eichler 2003; Zhang, Woosley & MacFadyen 2003; Zhang, Woosley & Heger 2004; Lazzati & Begelman 2005; Morsony, Lazzati & Begelman 2010) or, instead, the SJ could have an 'external' origin (Ghisellini et al. 2007).

Direct tests of the SJ model with available data, e.g. the search for a possible anticorrelation between $E_{\gamma,\rm iso}$ and $\theta_{\rm v}$ (Perna, Sari & Frail 2003; Lloyd-Ronning, Dai & Zhang 2004) or the statistical studies of the flux cumulative distribution of large GRB samples in the SJ model, did not provide definite evidence for this model (Nakar, Granot & Guetta 2004; Cui, Liang & Lu 2005). However, the presence of a structured jet is invoked to interpret some GRBs with a double jet break in their afterglow light curves (e.g. Enigmatic Radio Afterglow of GRB 991216 – Frail et al. 2000; GRB 030329 – Berger et al. 2003, Sheth et al. 2003; GRB 021004 – Starling et al. 2005). In these cases, a 'discrete' SJ model composed by a narrow jet surrounded by a wider cone was proposed (Peng, Königl & Granot 2005), possibly due to the interaction of the jet with the star cocoon (Ramirez-Ruiz, Celotti & Rees 2002; Vlahakis, Peng & Königl 2003; Lazzati & Begelman 2005).

Several GRB properties are affected by the jet structure: the achromatic break $t_{\rm break}$ in the afterglow light curve is smoother in the SJ model and it is related to $\theta_{\rm v}$ rather than $\theta_{\rm j}$ (Zhang & Meszaros 2002); different degree of polarization of the afterglow emission (Lazzati et al. 2004; Rossi et al. 2004) and different luminosity functions (LF) (and GRB rates) are expected in the two scenarios. The jet break measurements are hampered by the necessity of a follow-up of the afterglow emission until late times, by the smoothing induced by viewing angle effects (e.g. van Eerten & MacFadyen 2012) and by the contamination of the afterglow emission at late times by the possible supernova and host galaxy emission (e.g. Ghirlanda et al. 2007). Despite all these diagnostics, there is no concluding evidence yet of the real jet structure. On the other hand, the increasing number of bursts with measured redshift allows us to estimate the LF of GRBs with increasing confidence. We show in this paper how the jet structure affects the observed LF.

The most recent studies of the GRB LF are by Wanderman & Piran (2010) with a relatively large GRB sample, and by Salvaterra et al. (2012) with a relatively small but complete GRB sample. GRBs with measured redshift have typical isotropic equivalent luminosities in the range 10^{50-54} erg s^{-1}. At lower luminosities, the detection rate drops to only a few events which are, however, representative of a large local density of GRBs (e.g. Pian et al. 2006; Soderberg et al. 2006). Indeed, it has been suggested that these latter events could belong to a different GRB population (e.g. Daigne & Mochkovitch 2007; Virgili, Liang & Zhang 2009).

1.1 Structure of this work

In this paper, we first consider the low-luminosity (LL) GRBs to discuss if they can be accounted for by the extrapolation of the LF describing high-luminosity (HL) GRBs (Section 2). In this case, we would have an LF extending over seven orders of magnitude to be compared with different models. Then, we study four different possibilities.

(i) First, we consider the simplest model: all jets are uniform, with the same $\theta_{\rm j}$ and are seen always on-axis, but we assume that the jet had to punch the progenitor star before emerging, and in so doing it must spend $\sim 10^{51}$ erg. We derive the predicted LF in this case, and compare it to the data (Section 3.1.1).

(ii) Then, we allow $\theta_{\rm j}$ to vary as a function of the observed luminosity, but we still assume that all bursts are seen on-axis. Bursts of equal collimation-corrected luminosity, but of different $\theta_{\rm j}$ will have different isotropically equivalent luminosities $L_{\rm iso}$ (the smaller $\theta_{\rm j}$, the larger $L_{\rm iso}$). Also in this case, we can construct analytically the LF, and we compare it with the data (Section 3.1.2).

(iii) We consider the possibility that (some) GRBs can be detected even if observed off-axis, even if the jet is uniform. In fact, any GRB will emit not only within $\theta_{\rm j}$, but also outside, even if the corresponding radiation is not as relativistically boosted as the radiation inside the jet cone. The observable off-axis luminosity depends on the bulk Lorentz factor (the larger Γ, the dimmest the off-axis luminosity). The predicted LF for a single value of Γ and $\theta_{\rm j}$ can be derived analytically, allowing for an easy numerical computation of the LF with a distribution of Γ and $\theta_{\rm j}$. The latter is compared to the data (Section 3.2).

(iv) Finally, we consider structured jets, characterized by a power-law dependence of the radiated energy with the angle from the jet axis ($E \propto \theta^{-s}$) to find out if the data are consistent with this scenario, and for which slope s (Section 4).

We discuss our results in Section 5. In this paper, we assume a standard flat cosmology with $h = \Omega_\Lambda = 0.7$.

2 LONG GRB LUMINOSITY FUNCTION

The problem of deriving the luminosity function [LF – $\Phi(L)$] of GRBs has been approached by different authors (Firmani et al. 2004; Guetta, Granot & Begelman 2005; Natarajan et al. 2005; Daigne, Rossi & Mochkovitch 2006; Salvaterra & Chincarini 2007; Salvaterra et al. 2009, 2012; Jakobsson et al. 2012; Shahmoradi 2013; Howell et al. 2014) by convolving $\Phi(L)$ with the GRB formation rate $R_{\rm GRB}(z)$ (proportional to the cosmic star formation rate). The free parameters of the LF can be constrained by fitting the resulting model to the flux distribution of large GRB samples (e.g. the *Compton Gamma-ray Observatory* (*CGRO*)/BATSE population). Note that, in the GRB literature, it is customary to consider as cosmic evolution any (i.e. density, or luminosity, or both) evolution *in addition* to the one related to the evolution of the star formation rate. The main difficulty of these studies is accounting, in the model, for the selection effects which affect the true GRB population detected by any instrument. Recently, Salvaterra et al. (2012 – S12 hereafter) constructed a flux-limited sample of bright GRBs detected by *Swift*/Burst Alert Telescope (BAT) which resulted 95 per cent complete in redshift (BAT6). Similarly, Jakobsson et al. (2012) built the TOUGH sample, which extends to fainter luminosities, and derived the LF.

While the possible evolution of the LF or of the GRB formation rate with redshift is still a matter of debate, there seems to be a general consensus on the shape of the LF:

$$\Phi(L) \propto \begin{cases} \left(\frac{L}{L_{\rm c}}\right)^{-a}, & L \leq L_{\rm c} \\ \left(\frac{L}{L_{\rm c}}\right)^{-b}, & L > L_{\rm c} \end{cases}, \quad (1)$$

where $L_{\rm c}$ represents the break luminosity. S12 finds $a = 1.56^{+0.11}_{-0.42}$, $b = 2.31^{+0.35}_{-0.31}$, $L_{\rm c} = 2.5^{+6.8}_{-2.1} \times 10^{52}$ erg s^{-1} (68 per cent confidence intervals) for the case of no evolution of $\Phi(L)$. Similar results ($a = 1.52$, $b = 2.00$, $L_{\rm c} = 10^{52.5}$ erg s^{-1}) are obtained by Jakobsson et al. (2012). Howell et al. (2014) derive a smaller low luminosity index $a = 0.95 \pm 0.09$ and consistent $b = 2.59 \pm 0.93$, $L_{\rm c} = 0.8 \pm 0.43 \times 10^{52}$ erg s^{-1}.

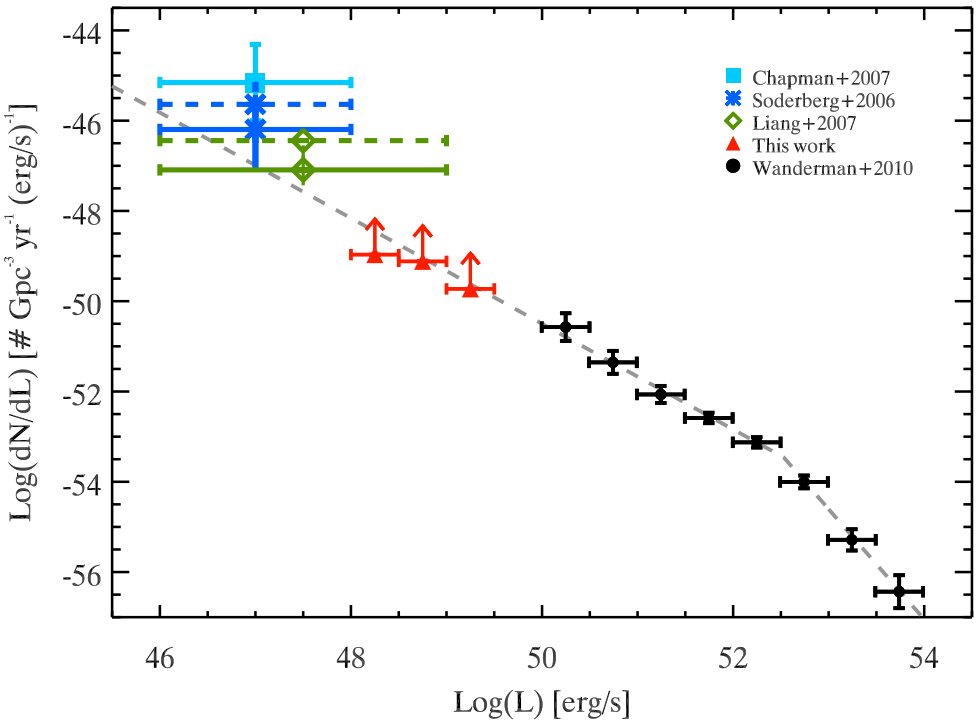

Figure 1. Long GRB LF representing the number of GRBs per unit volume, time and luminosity bin. Black symbols represent the discrete LF of WP10. The grey dashed line is the empirical fit of WP10 with a broken power law with $a = 1.2$, $b = 2.4$ and $L_c = 3.2 \times 10^{52}$ erg s^{-1}. The rate of LL GRBs is shown with different symbols according to the different sources in the literature: asterisk (Soderberg et al. 2006), diamond (Liang et al. 2007), filled square (Chapman et al. 2007). The Soderberg et al. (2006) and Liang et al. (2007) rates were calculated assuming a time bin corresponding to the *Swift* lifetime in 2006 (points with dashed horizontal bars). Since then, no other burst in the same luminosity bin has been discovered, so we added the rates corrected for the current *Swift* lifetime (points shown with solid horizontal bars). The lower limits on the rate of IL GRBs added in this work are shown with the filled (red) triangles.

2.1 HL GRBs

Wanderman & Piran (2010, WP10 hereafter) adopted a direct inversion method on the distribution of GRBs in the L–z space obtaining simultaneously $\Phi(L)$ and $R_{\rm GRB}$ independently.[1] They selected a sample of long[2] GRBs with spectroscopically measured redshift and isotropic equivalent luminosities $L_{\rm iso} \geq 10^{50}$ erg s^{-1} detected by BAT on board *Swift*. The derived LF is represented by a discrete series of data points (fig. 3 of WP10) in eight equal logarithmic bins of luminosity and can be represented by a broken power law with $a = 1.2^{+0.2}_{-0.1}$ and $b = 2.4^{+0.3}_{-0.6}$, with the break at $L_c = 10^{52.5 \pm 0.2}$ erg s^{-1} (note that WP10 use $\mathrm{d}N/\mathrm{dlog}\,L$, whereas we prefer to adopt $\mathrm{d}N/\mathrm{d}L = \mathrm{d}N/(L\ \mathrm{dlog}\,L)$ so that the WP10 slopes are here increased by 1).

These parameter values are consistent with those derived with the 'classical' approach described above. We normalized the LF at the local GRB rate $\rho_0 \simeq 1.3$ Gpc^{-3} yr^{-1} (WP10). Fig. 1 shows the data points of WP10 (black symbols) which cover the luminosity range between 10^{50} and 10^{54} erg s^{-1} and will be referred to as HL bursts hereafter. The best fit obtained by WP10 is shown as a grey long dashed line.

[1] This method relies on the assumption of no evolution of the GRB LF and rate with redshifts. See WP10 for the validity of this assumption.

[2] See Wanderman & Piran (2014) for the same method applied to short GRBs.

2.2 LL GRBs

At the low end of the luminosity distribution of GRBs, i.e. $L_{\rm iso} \sim 10^{46-48}$ erg s^{-1}, there are two events (GRB 980425 and GRB 060218) which have been detected in the local Universe and have been intensively studied as direct evidences of the massive star progenitor of long GRBs. Their luminosity is three orders of magnitude smaller than HL bursts, and their rate is larger (e.g. Soderberg et al. 2006). GRB 980425 ($z = 0.008$, associated with SN1998bw – Galama, Vreeswijk & van Paradijs 1998) was detected by *CGRO*/BATSE and had $L_{\rm iso} \sim 7 \times 10^{46}$ erg s^{-1} (as computed from its prompt emission spectrum – Jimenez, Band & Piran 2001). Similarly, GRB 060218 ($z = 0.0331$, associated with SN2006aj – Sollerman et al. 2006), detected by *Swift*/BAT, had $L_{\rm iso} \sim 1.3 \times 10^{47}$ erg s^{-1} (Campana et al. 2006).

The rate of these LL events can be computed as

$$\rho_{\rm LL} \simeq 4\pi \frac{N_{\rm LL}}{V_{\rm max} T \Omega}, \qquad (2)$$

where $V_{\rm max}$ is the maximum volume within which they could be detected by an instrument with an assigned sensitivity, with a field of view Ω and operating for a time T. Based on the two GRBs 980425 and 060218, Soderberg et al. (2006; see also Pian et al. 2006) derived the rate of LL events by conservatively averaging over $V_{\rm max}$ and Ω for different detectors (*Beppo*SAX/Wide Field Camera, *Hete–II*/Wide Field X-ray Monitor and *Swift*/BAT). They obtained a rate $\rho_{\rm LL} \sim 230^{+490}_{-190}$ Gpc^{-3} yr^{-1}. In the luminosity range 10^{46}–10^{48} erg s^{-1} occupied by these two GRBs and centred at $\langle L \rangle = 10^{47}$ erg s^{-1}, we convert this rate dividing it for the interval

Table 1. IL GRBs. [a]References for the redshift: (1) GCN #1554, Soderberg et al. (2002); (2) GCN #2482, Prochaska et al. (2003); (3) GCN #5387, Perley et al. (2006); (4) GCN #5161, Thoene, Fynbo, Sollerman et al. (2006); (5) GCN #13251, Tanvir et al. (2012); (6) GCN #14983, Leloudas et al. (2013); [b]References for the spectral parameters: (7) Sakamoto et al. (2004); (8) Bosnjak et al. (2014); (9) Sazonov et al. (2004); (10) Ulanov et al. (2005); (11) Troja et al. (2006); (12) Sakamoto et al. (2009); (13) Butler et al. (2007); (14) Zhang et al. (2012); (15) von Kienlin et al. (2014). [†]$E_{\rm peak}$ computed through the α–$E_{\rm peak}$ correlation of Sakamoto et al. (2009) for *Swift* GRBs (for GRB 051109B consistent also with the estimate of Butler et al. 2007).

GRB	z	Ref[a]	α	β	$E_{\rm peak}$ (keV)	P (ph cm^{-2} s^{-1})	ΔE (keV)	Ref[b]	$P_{\rm bol}$ (ph cm^{-2} s^{-1})	$L_{\rm iso}$ (erg s^{-1})	Instr.	$P_{\rm lim,\,bol}$ (ph cm^{-2} s^{-1})
020903	0.25	1	−1.0	–	3.37	2.8	[2–400]	7	6.52	4.86×10^{48}	*Hete–II*	3.0
031203	0.105	2	−1.63	–	144	2.2	[15–150]	8,9,10	17.9	10^{49}	*Integral*	3.0
051109B	0.08	3	−1.90	–	50[†]	0.5	[15–150]	11,12,13	9.43	1.64×10^{48}	*Swift*	1.3
060505	0.089	4	−1.8	–	239[†]	1.9	[15–150]	11	8.0	7.14×10^{48}	*Swift*	0.8
120422A	0.283	5	−1.94	–	53	0.6	[15–150]	14	11.35	2.7×10^{49}	*Swift*	2.5
130702A	0.145	6	−1.0	−2.5	20	7.03	[10–1000]	15	7.03	2.87×10^{49}	*Swift*	2.5

width obtaining $\tilde{\rho}_{\rm LL} \sim 2.3 \times 10^{-46}$ Gpc^{-3} yr^{-1} erg^{-1} s. This is represented by the (blue) asterisk in Fig. 1. Since $\rho_{\rm LL}$ has been computed in 2006, we have also corrected it (blue asterisk with solid horizontal bar in Fig. 1) for the larger time interval elapsed since the detection of these two LL events. These results are consistent with numerical studies: Virgili et al. (2009) estimate $\rho_{\rm LL}$= 200 Gpc^{-3} yr^{-1} for events with $\langle L \rangle = 10^{47}$ erg s^{-1} based on the BATSE GRB population. A slightly larger rate $\rho_{\rm LL} \sim 700 \pm 360$ Gpc^{-3} yr^{-1} (shown by the cyan filled square symbol in Fig. 1) has been obtained by Chapman et al. (2007) from the cross-correlation of a subsample of low-fluence smooth single-peaked BATSE bursts with nearby galaxies. We show this rate only for consistency with the others but we do not take it into account in the calculations since it is derived in a different way with respect to Soderberg et al. (2006). Liang et al. (2007) also derived $\rho_{\rm LL} = 325^{+352}_{-177}$ Gpc^{-3} yr^{-1} (shown by the green diamond symbol in Fig. 1 and also corrected for the lifetime of *Swift*).

2.3 Intermediate-luminosity GRBs

In the intermediate luminosity (IL) range between HL and LL (see Fig. 1), we can add some constraints. We have searched all GRBs with measured redshift[3] z and with $L_{\rm iso} \in [10^{48}, 10^{50}]$ erg s^{-1}. In addition to z, we also required that $L_{\rm iso}$ is well determined: this is possible when the spectrum at the peak of the light curve has been fitted over a wide enough energy range as to constrain its peak energy. Indeed, in these cases it is possible to compute the bolometric isotropic luminosity. We adopted the same method described for LL (from Soderberg et al. 2006) to compute $\rho_{\rm IL}$ in three luminosity bins, using the following bursts: (i) GRB 051109B with $L_{\rm iso} \in [10^{48}, 3 \times 10^{48}$ erg s$^{-1}]$, (ii) GRB 020903, 031203, 060505 with $L_{\rm iso} \in [3 \times 10^{48}, 10^{49}$ erg s$^{-1}]$ and (iii) GRB 120422A, 130702 with $L_{\rm iso} \in [10^{49}, 3 \times 10^{49}$ erg s$^{-1}]$.

We have collected the prompt emission spectral parameters and flux of these bursts (reported in Table 1 – Columns 4–8) through which we have computed their bolometric flux (Column 11 in Table 1). Three different instruments were involved in triggering these events (Column 10 in Table 1), and we considered the following instrumental parameters: $\Omega = 1.33$ sr and $T = 8$ yr for *Swift*, $\Omega = 0.1$ sr and $T = 10$ yr for *Integral* and $\Omega = 0.802$ sr and $T = 4$ yr for *Hete–II*. The last column in Table 1 reports the limiting flux of the corresponding detectors as computed by Band (2002, 2006) which depends on the burst peak spectral energy $E_{\rm peak}$ (in the observer frame). $P_{\rm lim}$ as computed by Band (2002, 2006) in the 1–1000] keV observed energy band is used to compute the maximum distance (and therefore $V_{\rm max}$) out to which these events could have been detected. With the same method adopted for LL bursts, we could derive a rate $\rho_{\rm IL}$ for IL events. These rates should be considered as lower limits: we only selected GRBs with measured redshifts and well-constrained spectral parameters. These are most likely only a fraction of the bursts, with similar luminosities, which effectively triggered the corresponding detector. These rates are shown by the (red) triangles in Fig. 1.

Finally, Fig. 1 shows the LF of HL bursts (data points from WP10 – black symbols), IL bursts (lower limits – red triangles) and LL bursts (coloured symbols – references in the caption). The grey dashed line represents the LF fitted by WP10 to their data points (only HL bursts) and it can be noted that its extrapolation to low luminosities is consistent with both the lower limits of IL bursts and the rate of LL events. This is a direct indication that LL and HL have a common progenitor, i.e. they form a *unique population*. Apparently there is no need to invoke a different origin for the LL events as they are consistent with the extension to low luminosities of the LF of HL bursts. Based on this evidence, in the following we compare the empirical LF with model predictions for different jet configurations.

3 UNIFORM JET

In this section, we derive the analytic expression of the LF under the assumptions of UJ, e.g. we assume that the energy per unit solid angle ϵ and the initial bulk Lorentz factor Γ_0 are constant within the jet, and zero outside.

3.1 Jet break-out energy

To be observed, the jet must emerge from the progenitor star. This implies that a minimum central engine duration is required for a jet to successfully escape the progenitor star. Bromberg et al. (2012) derived interesting consequences from this simple consideration, concerning the GRB duration distribution. If the central engine lasts much longer than the time necessary for the jet to drill through the star (break out time), the resulting GRB will be a long one. If the central engine duration is comparable to the break out time, but slightly longer, the GRB will be short. As a consequence, Bromberg et al. (2012, 2013) estimated the fraction of short GRBs produced by collapsars and revised the separation of long/short events.

The same argument can be applied to the energetics. In a recent work, Kumar & Smoot (2014) find that the minimum energy required to excavate the star envelope must be at least the energy

[3] http://www.mpe.mpg.de/~jcg/grbgen.html

contained in the cocoon. Based on Mészáros & Rees (2001), we assume that the energy associated with the cocoon is $E_* \simeq 10^{51}$ erg.

Therefore, if the inner engine provides enough energy $E_{\rm kin} > E_*$, the jet can escape the star and the GRB can be observed. The 'residual' energy of the burst will be $E_{\rm kin} - E_*$. If $E_{\rm kin} \gg E_*$, a normal HL burst is observed, while LL events are those with $E_{\rm kin}$ only slightly larger than E_*. We show below that, likewise to the duration distribution (Bromberg et al. 2012), also the energy distribution should be flat below the characteristic E_*.

Assume that the central engines of GRBs provide a total kinetic energy distributed as $P(E_{\rm kin}) = {\rm d}N(E_{\rm kin})/{\rm d}E_{\rm kin} \propto E_{\rm kin}^{-k}$. Of the total kinetic energy $E_{\rm kin}$ produced by the central engine, only $E_{\rm kin} - E_*$ is available, left after the jet has escaped the progenitor star. Moreover, only *a fraction* η of the residual kinetic energy $E_{\rm kin} - E_*$ can be converted into radiation (η is typically a few per cent in the standard internal shock model – Rees & Meszaros 1994).

If $E_\gamma = \eta(E_{\rm kin} - E_*)$ is the energy converted into radiation, we can define its isotropic equivalent as

$$E_{\rm iso} = \frac{\eta(E_{\rm kin} - E_*)}{1 - \cos\theta_{\rm j}}, \tag{3}$$

where $\theta_{\rm j}$ is the jet opening angle. The relation between $P(E_{\rm kin})$ and $P(E_{\rm iso})$ is

$$P(E_{\rm iso}) = P(E_{\rm kin})\frac{{\rm d}E_{\rm kin}}{{\rm d}E_{\rm iso}}. \tag{4}$$

To pass from the energy function to the LF, we take advantage of the fact that the distribution of the rest-frame duration of GRBs peaks at 25 s. This is true also for the bursts used by WP10. Assuming that the light curve of the prompt emission can be approximated by a triangular shape, we have $E_{\rm iso} \approx (t \times L_{\rm iso})/2$.

Then, the LF in the UJ model is

$$P(L_{\rm iso}) = P(L_{\rm kin})\frac{{\rm d}L_{\rm kin}}{{\rm d}L_{\rm iso}} = L_{\rm kin}^{-k}\frac{1-\cos\theta}{\eta}$$
$$\propto \frac{(1-\cos\theta_{\rm j})}{\eta}\left[\frac{L_{\rm iso}(1-\cos\theta_{\rm j})}{\eta} + L_\star\right]^{-k}, \tag{5}$$

where L_* is the collimation corrected (i.e. 'true') *kinetic* luminosity necessary to punch the star, while $L_{\rm iso}$ is the observed, isotropically equivalent *radiative* luminosity. Equation (5) is the LF of *all* bursts, including the ones not pointing at us. If all bursts have the same $\theta_{\rm j}$, we will see only a fraction $(1 - \cos\theta_{\rm j})$ of them, independent of luminosity. Therefore, the observed LF is

$$P(L_{\rm iso}) \propto \frac{(1-\cos\theta_{\rm j})^2}{\eta}\left[\frac{L_{\rm iso}(1-\cos\theta_{\rm j})}{\eta} + L_\star\right]^{-k}. \tag{6}$$

Only those engines providing $L > L_*$ will produce a successful GRB and build up the $P(L_{\rm iso})$ distribution: if $L \gg L_*$, then $P(L_{\rm iso}) \propto L_{\rm iso}^{-k}$, whereas for $L \lesssim L_*$ the LF is flat:

$$P(L_{\rm iso}) \propto \begin{cases} {\rm const}, & L_{\rm iso} \ll \eta L_\star/(1-\cos\theta_j) \\ L_{\rm iso}^{-k}, & L_{\rm iso} \gg \eta L_\star/(1-\cos\theta_j) \end{cases}. \tag{7}$$

The transition between these two regimes corresponds to a characteristic luminosity, i.e. $L_{\rm iso} \sim \eta L_*/(1 - \cos\theta_{\rm j})$.

3.2 UJ observed in-jet [$\theta_{\rm v} < \theta_{\rm j}$]

Independently from the jet structure (UJ or SJ), one important parameter affecting the observed properties of GRBs is the viewing angle $\theta_{\rm v}$, i.e. the angle between the observer line of sight and the jet axis. In the UJ model, we first assume that the emission can be seen only if the observer line of sight intercepts the jet aperture angle, i.e. $\theta_{\rm v} \leq \theta_{\rm j}$. This is a good approximation if the bulk Lorentz factor of the prompt phase Γ_0 is relatively large, i.e. $1/\Gamma_0 \ll \theta_{\rm j}$.

3.2.1 *Unique jet opening angle* $\theta_{\rm j}$

Assume that all GRBs have the same $\theta_{\rm j}$. $P(L_{\rm iso})$ in equation (6) represents the LF of the *observed* GRBs. The *total* LF is given in equation (5). The factor $(1 - \cos\theta_{\rm j})$ is in this case constant, and can be absorbed in the normalization of equation (6). Fig. 2 shows the fit of the LF with the model of equation (6). We fit the HL rates (black symbols) and the LL rate (blue asterisk) as derived by Soderberg et al. (2006 – corrected in this work for the elapsed time, see Section 2).[4] The lower limits of IL bursts (red triangles in Fig. 2) are used only for a consistency check of the fitted model.

Fixing $L_* = 10^{50}$ erg s^{-1}, the free parameters are the normalization, the slope k and the characteristic luminosity $L_*\eta/(1 - \cos\theta_{\rm j})$. Since the model depends on the ratio between η and $(1 - \cos\theta_{\rm j})$, there is degeneracy between these two quantities. The fit can constrain this ratio rather than the two factors independently. We consider two cases:

(i) η=0.2 (as typically found from the modelling of the GRB afterglows – e.g. Panaitescu & Kumar 2002): the fit is shown by the solid cyan line in Fig. 2. HL bursts can be reproduced with a unique LF which has a slope $k = 1.62 \pm 0.08$ (1σ confidence) and is also marginally consistent with the IL lower limits. The fit has $\chi^2 = 33.5$ for 6 degrees of freedom (dof) corresponding to a goodness of fit probability of 8×10^{-6}. However, the LL bursts cannot be reproduced by this model. Indeed, the characteristic luminosity $L_*\eta/(1 - \cos\theta_{\rm j})$, with $\eta = 0.2$ and $L_* = 10^{50}$ erg s^{-1}, corresponds to $\sim 2 \times 10^{49}/(1 - \cos\theta_{\rm j})$ erg s^{-1}. This expression has a minimum for $\theta_{\rm j} = 90^\circ$. In this case, all GRBs would be isotropic and still LL events should be a different population;

(ii) $\theta_{\rm j} = 5^\circ$ (i.e. corresponding to the typical opening angle of GRBs – Frail et al. 2001; Ghirlanda et al. 2007): the fit is shown by the dashed green line in Fig. 2 and can reproduce all the bursts (with a $\chi^2 = 16$ for 6 dof, i.e. probability 0.01). The resulting $k = 1.49 \pm 0.08$ is consistent with the previous one, but the efficiency $\eta \sim 10^{-5}$ is unreasonably low.

We have verified that the above results are independent from the choice of the particular value for L_*: if we fix this parameter to any value $[10^{49}, 10^{51}]$ erg s^{-1}, we still find an unreasonably low efficiency $\eta < 10^{-5}$ for 'reasonable' $\theta_{\rm j}$; or too large $\theta_{\rm j}$ for 'reasonable' efficiencies. This is shown in the inset of Fig. 2 where all the curves saturate at 90° (for the three different choices of L_*) for $\eta > 0.01$.

We conclude that the UJ model (assuming a unique angle for all bursts) does not reproduce the entire LF (from LL to HL bursts).

3.2.2 *Jet angle depending on luminosity* [$\theta_{\rm j}$(L)]

The assumption made in the previous section, that all GRBs have the same jet angle, may be relaxed. Indeed, there is the possibility that the LL bursts have wide opening angles to account for their

[4] We use only the LL rate of Soderberg et al. (2006). The rate of Liang et al. (2007), though derived in a similar way, does not average different satellites' sensibilities as in Soderberg et al. (2006). The rate of Chapman et al. (2007) is not considered because it is inferred from a correlation of GRBs with local galaxies.

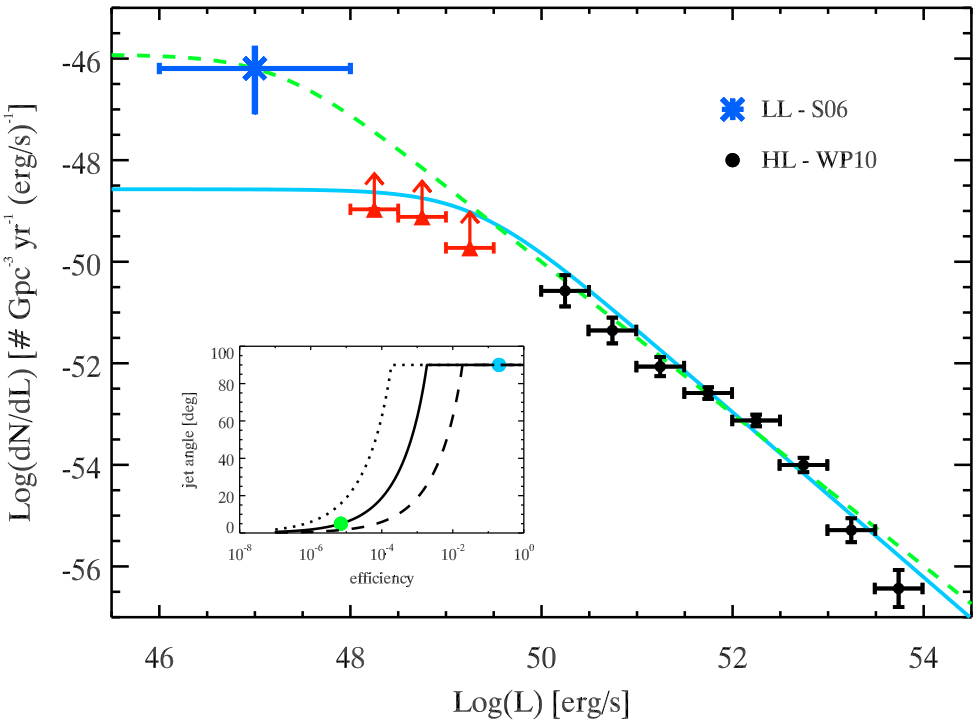

Figure 2. LF fitted with the UJ model (equation 6) with fixed opening angle. For the models shown in the main plot (solid cyan and dashed green curves), $L_* = 10^{50}$ erg s^{-1} is fixed. The solid cyan line shows the case with $\eta = 0.2$ (which gives $\theta_j = 90^\circ$) and the dashed green line is the case with $\theta_j = 5^\circ$ (which gives $\eta \sim 10^{-5}$). Inset: curves showing the degeneracy of the model in the angle and efficiency parameters. Dotted, solid and dashed curves correspond to different choices of $L_* = 10^{49}, 10^{50}, 10^{51}$ erg s^{-1}, respectively. The green and cyan dots show the choice of η and θ_j corresponding to the model curves shown in the main panel, respectively.

low luminosity. If the luminosity range of the LF is due to the range of opening angles, one should expect an anticorrelation between L_{iso} and θ_j. Indeed, it has been shown that such a relation exists for GRBs with measured θ_j (e.g. Lloyd-Ronning et al. 2004; Firmani et al. 2005; Ghirlanda, Ghisellini & Firmani 2005).

The peak energy E_{peak} of GRBs is correlated with the isotropic energy E_{iso} as $E_p = k_A E_{iso}^A$ (Amati et al. 2002) with $A \sim 0.5$ (a similar correlation exists with the isotropic luminosity: $E_p = k_Y L_{iso}^Y$ – Yonetoku et al. 2004). The slopes of these two correlations are similar $A \sim Y \sim 0.5$.

If E_{iso} is corrected for collimation, namely $E_\gamma = E_{iso}(1 - \cos\theta_j)$, a tighter and steeper correlation $E_p = k_G E_\gamma^G$ (Ghirlanda et al. 2004) is found. The slope depends on the density profile of the circumburst medium, being $G = 0.7$ for a homogeneous density and $G = 1$ for a wind profile (Nava et al. 2006). Since the E_p–E_{iso} and E_p–E_γ correlations differ for the collimation factor (i.e. $1 - \cos\theta_j$), their different slopes suggest that there is a relation between the average jet opening angle and the energy of GRBs: more energetic bursts should have a smaller θ_j.

We can derive this relation by combining the correlations

$$1 - \cos\theta_j = \left(\frac{k_A}{k_G}\right)^{1/G} E_{iso}^{(A-G)/G} = C L_{iso}^{-\xi}, \quad (8)$$

where $\xi = (G - A)/G$. The typical duration, assumed $t = 25$ s (rest frame) to convert energetics to luminosities, has been incorporated in the normalization constant C. This relation also establishes that there is a characteristic minimum luminosity $L_{iso,min} \sim 7 \times 10^{46}$ erg s^{-1} corresponding to $\theta_j = 90^\circ$.

Since θ_j is not constant, it is convenient to find the LF of all bursts, including the ones not pointing at us, i.e. using equation (5). The LF then becomes

$$P(L_{iso}) \propto \frac{C(1-\xi)L_{iso}^{-\xi}}{\eta}\left(\frac{CL_{iso}^{1-\xi}}{\eta} + L_\star\right)^{-k}, \quad (9)$$

where the factor $(1 - \xi)$ comes from the derivative dL_{kin}/dL_{iso} in which now also the collimation factor depends on L_{iso}. At low L_{iso}, $N(L_{iso}) \propto L^{-\xi}$, while at large L_{iso}, $N(L_{iso}) \propto L^{-\xi - k(1-\xi)]}$. The break is at $L_{iso} \sim (\eta L_*/C)^{1/(1-\xi)}$.

In Fig. 3, the corrected points (black dots and red triangles) are shown together with the observed ones (grey dots): the higher the luminosity, the larger is the applied correction, according to equation (8). Below a limiting L_{iso}, the opening angle becomes larger than 90° and we do not apply the correction any longer. Since smaller angles correspond to larger L_{iso}, the LF of all GRBs is flatter than the observed one.

Fixing $L_* = 10^{50}$ erg s^{-1}, the fit favours an efficiency $\eta = 1$ (pegged to its maximum value) which is unrealistic (e.g. there would be no energy left for the afterglow emission). Similarly to the previous case, changing L_* by a factor 10 still gives $\eta = 1$. This is due to the degeneracy between η and L_*. Only for $L_* \geq 10^{52}$ erg s^{-1}, we find reasonable values of η. Therefore, we decided to show in Fig. 3 the fit with both η and L_* fixed to their typical values (0.2 and 10^{50} erg s^{-1}, respectively) (cyan solid line). The fit is consistent with the lower limits of the IL bursts (triangles in Fig. 3) and marginally consistent with the LL bursts. Setting $A = 0.5$, $G = 1$, we have $\xi = 0.5$, which is the slope at low luminosities. The slope of the distribution of energies provided by the inner engine found by the fit is $k = 1.5 \pm 0.15$, corresponding to a high-luminosities slope $\xi + k(1 - \xi) \simeq 1.25$ for $\Phi(L)$. We stress that 'finding the best

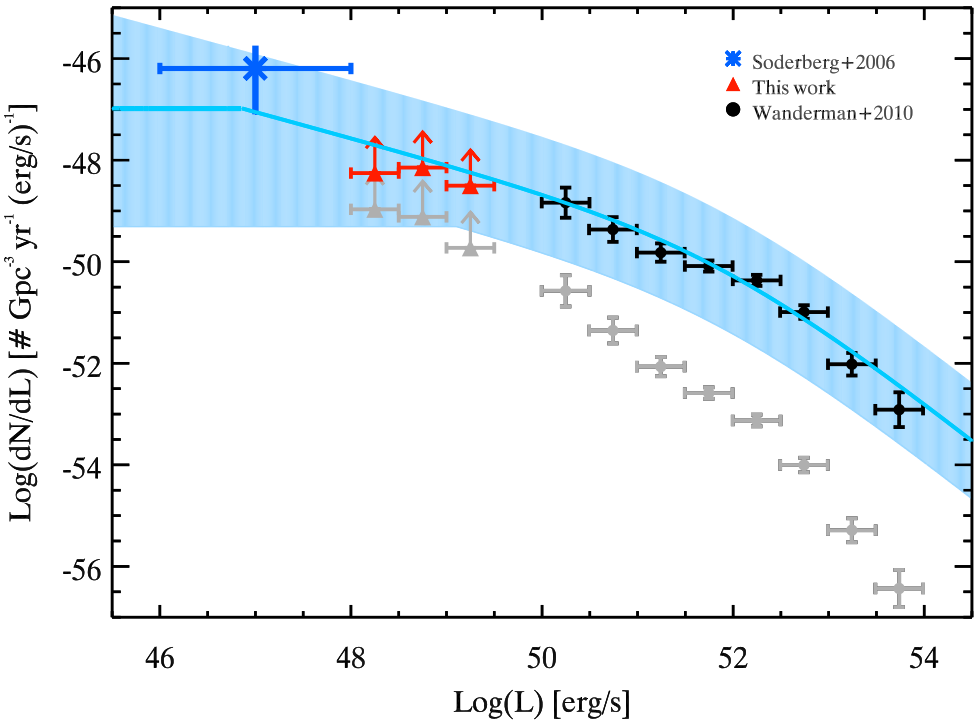

Figure 3. UJ with jet angle dependent from the luminosity. The LF of the entire GRB population (i.e. corrected for the collimation factor, which depends on the luminosity in this case) is shown by the black symbols. Original points (grey symbols) are also shown. The model is shown by the solid cyan line and the 3σ confidence interval of the model, obtained accounting for the scatter of the θ_j–L_{iso} correlation (see text) is shown by the azure shaded region.

fit' is here only a formal procedure: to the errors associated with the data points, we should in fact add the uncertainties about the E_p–E_{iso} and E_p–E_γ correlations, that have a scatter of 0.22 and 0.12 dex, respectively. Fig. 3 shows (shaded region) the 3σ boundaries of the LF obtained accounting for the scatter of these correlations in deriving the correlation of equation (8). The LL point is at the border of this confidence interval.

3.3 UJ observed in- and out-jet [$\theta_v \lesssim \theta_j$]

In the previous subsections, we assumed that we can see the prompt emission of GRBs only if we are within the jet opening angle, $\theta_v \leq \theta_j$, i.e. that off-axis observers see no emission. This implies large bulk Lorenz factors, i.e. $\Gamma \gg 1/\theta_j$. However, the slope of the LF found by WP10 below the break (dashed line in Fig. 1) is $\sim$1.25. This slope can be predicted in the case of UJ observed off-axis. To see this, consider a population of bursts $N(L_{iso,on})$ that have the same $L_{iso,on}$ when observed on axis. The number of bursts seen at different viewing angles will depend on the corresponding solid angle, and they will be observed with a reduced (de-beamed) luminosity L (see Ghisellini et al. 2006, for GRBs; Urry & Shafer 1984; Celotti et al. 1993, for blazars):

$$N(L, L_{iso,on})\mathrm{d}L = \frac{\mathrm{d}\Omega}{2\pi} \rightarrow N(L, L_{iso,on}) = \left(\frac{\mathrm{d}L}{\mathrm{d}\cos\theta}\right)^{-1}. \quad (10)$$

The observed luminosity is the sum of the contributions of different portions of the emitting surface, each observed under a different angle (Ghisellini et al. 2006):

$$L(\theta_v) = \int_{\max(0,\theta_v-\theta_j)}^{\theta_v+\theta_j} \Delta\phi\, \delta^4\, L'\, \sin\theta\, \mathrm{d}\theta, \quad (11)$$

where L' is the comoving luminosity per unit solid angle (which is assumed constant throughout the entire jet surface), θ is defined as the angle between the line of sight, $\delta \equiv [\Gamma(1 - \beta\cos\theta_v)]^{-1}$ is the relativistic Doppler factor and each emitting element of the jet and $\Delta\phi$ takes into account the geometry of the emitting surface. If the line of sight coincides with the jet axis, the emitting surface is a circular corona so that $\Delta\phi = 2\pi$, while for off-axis observers this is a portion of circular corona which depends on θ_v (Ghisellini & Lazzati 1999):

$$\Delta\phi = \begin{cases} 2\pi & \text{if } \theta < \theta_j - \theta_v \\ \pi + 2\sin\left(\frac{\theta_j^2-\theta_v^2-\theta^2}{2\theta_v\,\theta}\right) & \text{if } \theta \geq \theta_j - \theta_v \end{cases}. \quad (12)$$

The right-hand panel of Fig. 4 shows the LF for different choices of θ_j and Γ. According to the different scaling of L with θ_v, we have different slopes of the LF, which can be easily explained.

Small angles. $\theta_v < \theta_j$ – the observed luminosity increases only slightly by decreasing θ_v. This describes the HL end of the LF, in which $N(L)$ corresponds to the GRBs observable within θ_{jet} (see the right-hand panel of Fig. 4).

Intermediate angles. $\theta_j < \theta_v \lesssim 2\theta_j$ – equation (11) shows that the luminosity depends on the bulk Lorentz factor Γ, on the jet aperture angle θ_j and L'. Assuming $L' = 10^{49}$ erg s^{-1}, Fig. 4 (left-hand panel) shows how $L(\theta_v)$ depends on the different choices of θ_j and Γ. For large Γ, the observed luminosity drops by a large factor when θ_v becomes slightly larger than θ_j. This drop is smoother for smaller Γ. For $\theta_j < \theta_v \lesssim 2\theta_j$ (namely, within the 'jump', and before reaching the regime $L \propto \delta^4$), we can approximate the scaling of the

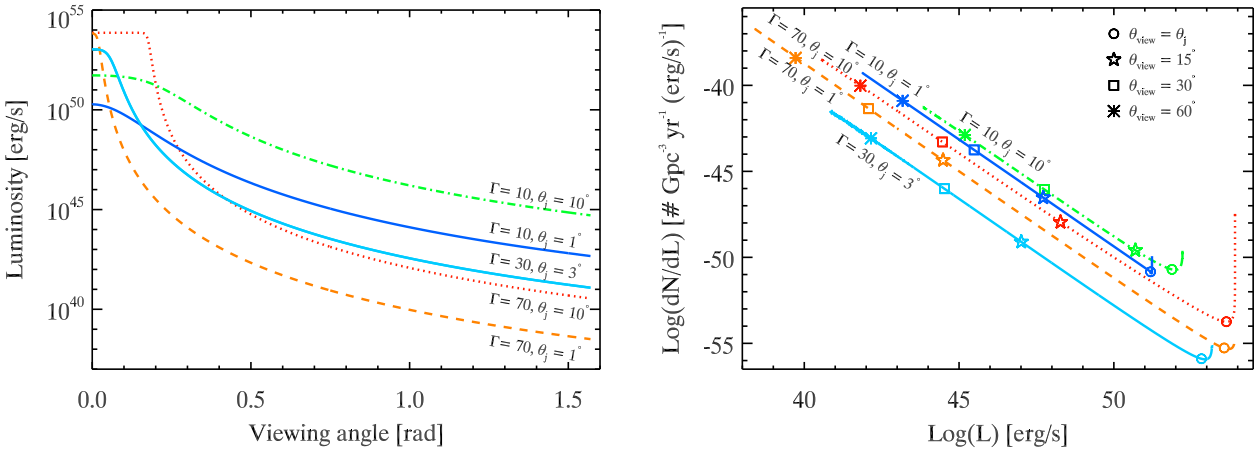

Figure 4. Left-hand panel: luminosity as a function of the viewing angle for different combinations of the bulk Lorentz factor Γ and jet opening angle θ_j. The comoving frame luminosity L' is the same for all curves. The different lines (colours) show different assumed combinations of θ_j and Γ. For all the curves, we have assumed $L' = 10^{49}$ erg s^{-1}. Right-hand panel: LF corresponding to the different assumptions of θ_j and Γ of the right-hand panel. The different symbols show different viewing angles as detailed in the labels.

luminosity as $L \propto \theta_v^{-f}$. According to equation (10), we have

$$N(L) \propto \left[\frac{dL}{\sin\theta d\theta}\right]^{-1} \propto \theta^{(f+2)} \propto L^{-(1+2/f)}, \quad \theta_j < \theta \lesssim 2\theta_j. \tag{13}$$

Note that the slope $1 + 2/f$ tends to unity for large f.

Large angles. $\theta_v \gg \theta_j$ – when $\theta_v \gg \theta_j$, the burst can be considered to have a mono-directional velocity, along the jet axis. In this case, the observed luminosity is proportional to δ^4. Therefore, $(dL/d\cos\theta)^{-1} \propto \delta^{-5} \propto L^{-5/4}$ [this results is general, as demonstrated by Urry & Shaefer (1984): for beaming amplification factors $L \propto \delta^p$, the resulting LL branch of the observed LF $N(L) \propto L^{-(1+1/p)}$].

As a first approximation, consider unique values of Γ and θ_j for all GRBs. The shapes of the corresponding LF are shown in Fig. 4 for different combinations of these two parameters, assuming a value of $L' = 10^{49}$ erg s^{-1}. The LF is a power law with a slope $-5/4$ which smoothly turns into a peak at high luminosities corresponding to the maximum observable luminosity. The LF of GRBs shown in Fig. 1 is consistent with a power law of slope -1.2 (WP10) and breaks into a steeper (-2.4) power law for $L_{iso} > 10^{52.5}$ erg s^{-1}. Therefore, there is very good agreement between the theoretical LF slope (Fig. 4) and the observed one below $10^{52.5}$ erg s^{-1} (Fig. 1). If we assume that the break luminosity corresponds to $L_{iso,on}$, i.e. of GRBs seen within the cone of their jet (i.e. those making the peak of the LF curves in Fig. 4), the true rate of GRBs can be computed as $N_{tot} = N_{obs}/(1 - \cos\theta_j)$ (where N_{obs} is the rate corresponding to the break of the LF of Fig. 1). Assuming that only ~ 0.3 per cent of SNIb/c produce GRBs (e.g. Ghirlanda et al. 2013), we estimate $\theta_j \sim 4°$. The other two parameters Γ and L' of the model can be constrained requiring that the integral of the LF corresponds to $N_{tot} \sim 100$ GRBs yr^{-1} Gpc^{-3}.

Still the model is not representative of the real data points, since there is the peak of the LF at the maximum luminosity (i.e. corresponding to the bursts observed within the jet aperture angle). In order to smooth this peak and obtain a break in the LF model, we introduce some dispersions of the values of Γ and θ_j. We find good agreement with the data as shown in Fig. 5 by the solid line assuming θ_j centred around 3° with a log-normal dispersion of width 0.2 and Γ centred at a value of 30 with a lognormal dispersion of width 0.14.

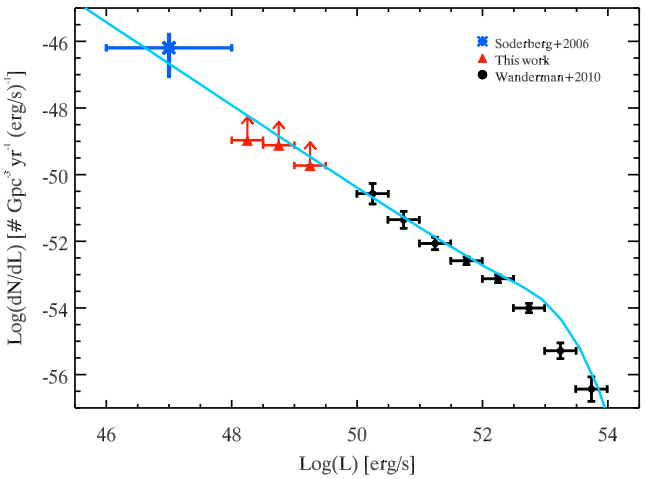

Figure 5. UJ observed in and out (ref Section 3.3).

4 STRUCTURED JET

In this section, we investigate the case of a structured jet, assuming that all burst have an identical structure, and that their observed properties are only due to the viewing angle θ_v. We assume that the distribution of the energy per unit solid angle $\epsilon(\theta)$ is constant within a core of small aperture θ_c and distributed as a power law at larger angles:

$$\epsilon(\theta) = \begin{cases} \epsilon_c & \text{if } \theta \le \theta_c \\ \epsilon_c \left(\frac{\theta}{\theta_c}\right)^{-s} & \text{if } \theta > \theta_c \end{cases}, \tag{14}$$

where ϵ_c is the energy per unit solid angle within the core of the jet. The integral of $\epsilon(\theta_v)$ is the total jet energy E which is a free parameter. Different jet structures have been considered from $s = 2$ (Rossi et al. 2002) to steeper structures (Zhang & Meszaros 2002 considered also the limit of a Gaussian jet). In the following, s is a free parameter. We define the energy observed at a certain θ_v as $E_{iso}(\theta_v) = 4\pi\eta\epsilon(\theta_v)$ and assuming a typical duration we can define

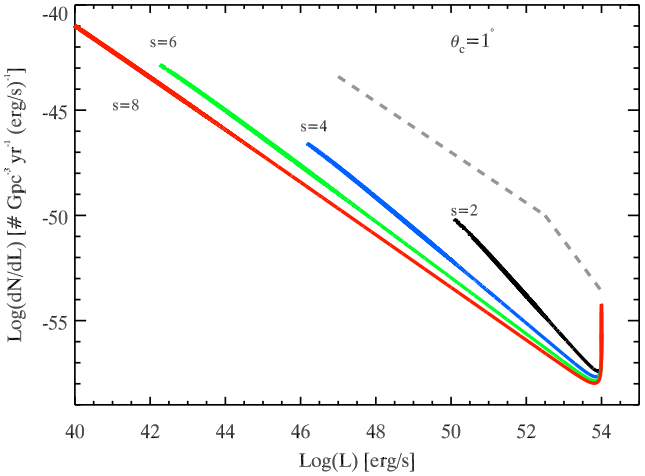

Figure 6. SJ model (solid lines) for different values of the power-law energy structure slope s (as labelled) assuming a core angle of 1°. The dashed grey line shows the observed LF (arbitrarily rescaled for clarity) of WP10 extending from LL to HL.

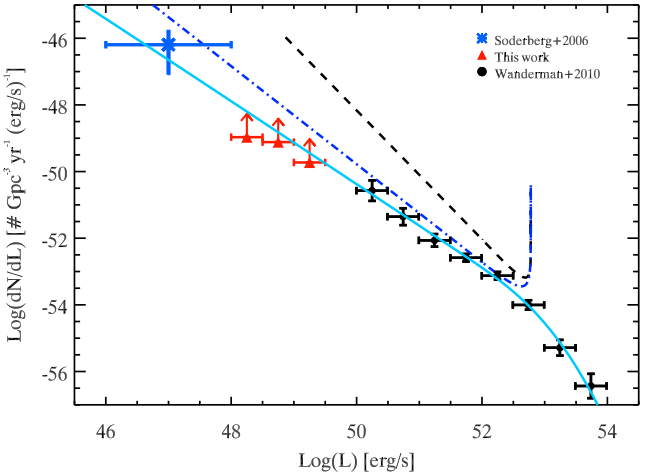

Figure 7. SJ model assuming a jet core energy per unit solid angle $\epsilon_c = 6 \times 10^{52}$ erg with a dispersion (lognormal) around this value with σ=0.5, $s = 8.1$ and $\theta_c \sim 5°$. For comparison are also shown the LF obtained with $s = 2$ and 4 (from Fig. 6) by the dashed and dot–dashed lines, respectively.

the luminosity as $L_{iso}(\theta_v) \propto \epsilon(\theta_v)$. For $\theta_v \leq \theta_c$, this corresponds to the maximum luminosity $L_{iso,max} \propto \epsilon_c$. The minimum luminosity is for $\theta_v = \pi/2$. From equation (14), the ratio between the maximum and minimum luminosity is $L_{max}/L_{min} = (\pi/2\theta_c)^s$: the extension of the resulting LF is set by the slope s and the jet core θ_c. Since the observed LF of GRBs (including HL and LL bursts) extends over seven orders of magnitudes (from 10^{47} to 10^{54} erg s^{-1}), we derive the limit $s \gtrsim 7/\log[\pi/(2\theta_c)]$. A typical core angle $\theta_c = 1°$ (Zhang et al. 2004; Lazzati & Begelman 2005) implies $s > 3.6$, thus excluding the $s = 2$ case which is instead what required by the clustering of the collimation-corrected energies of GRBs (Frail et al. 2001).

The LF of the SJ results

$$P(L_{iso}) \propto \sin\left\{\left(\frac{L_{iso}}{L_{iso,max}}\right)^{-1/s}\theta_c\right\}\left(\frac{L_{iso}}{L_{iso,max}}\right)^{-1-(1/s)}$$
$$\approx \theta_c\left(\frac{L_{iso}}{L_{iso,max}}\right)^{-(1+2/s)} \quad (15)$$

since the argument of the sine is always small for reasonable values of θ_c. The slope of the LF depends on the shape of the jet structure s which also regulates the extension of the LF (i.e. the ratio of the minimum and maximum observable luminosity) as shown by the different curves of Fig. 6. Formally, a slope $a = 1.25$ of the observed LF of Fig. 1 we get a typical value of $s = 8$. The upturn at large luminosities shown in Fig. 6 corresponds to the jets observed within the core which all have the same luminosity. Instead, the observed LF (Fig. 1) is steeper after a break corresponding to $L_{iso} \sim 3 \times 10^{52}$ erg s^{-1}. To reproduce this smooth break, we introduce some dispersion of the parameters. Fig. 7 shows that we can reproduce the LF if we assume a jet core energy per unit solid angle $\epsilon_c = 6 \times 10^{52}$ erg with a dispersion (lognormal) around this value with σ=0.5, s = 8.1 and $\theta_c \sim 5°$. The obtained LF is also consistent with the lower limits corresponding to the IL bursts.

5 DISCUSSION AND CONCLUSIONS

Due to the increased capability to measure the redshift of long GBRs, we have now better determination of their LF, and indeed the results of different groups and of different methods start to converge. The LF can be modelled as a broken power law, with slopes ∼1.2–1.5 and $b > 2$, and a break above 10^{52} erg s^{-1}. The degree of cosmic evolution is instead still uncertain (see e.g. S12). Another controversial issue concerns LL GRBs. We have observed very few of them, but their vicinity points to a very large rate. From what we find, they lie on the extrapolation of the LF that describes HL events. This suggests that LL and HL bursts belong to the same population. LL bursts have luminosities of $\sim 10^{47}$ erg s^{-1} and therefore extend the range of observed GRB luminosities to seven orders of magnitude. Note that the LF reconstructed in this work (Fig. 1) is consistent down to the lowest luminosities with a broken power-law model. These data still allow for the existence of a cut-off at even lower luminosities (Natarajan et al. 2005; Campisi, Li & Jakobsson 2010; Cao et al. 2011). Is the very large range of observed luminosities produced by the different intrinsic GRB power? Or is it, instead, the result of viewing the same intrinsic phenomenon under different lines of sight? We here discuss our findings, that are summarized in Table 2.

(i) If the jets of GRBs are homogeneous and have a typical opening angle, then the observed luminosity is proportional to the energetics of the bursts after it has spent part of its initial energy to punch the progenitor star. This implies that the LF must be flat at low luminosities, and this contradicts the data. Our conclusion is that we can exclude this simple case.

(ii) We have then examined the case of a homogeneous jet, but with a jet angle that is related to the GRB energetics: smaller θ_j correspond to larger E_{iso} and L_{iso}. Since LL bursts have larger θ_j, the probability that they intercept our line of sight is greater then that for HL bursts: therefore, the fraction of GRBs that we detect at lower luminosities is greater than at large luminosities. If the 'true' LF is flat, the observed LF is instead decreasing towards larger L_{iso} with a slope that depends on the chosen relation between θ_j and L_{iso}. The latter can be inferred by the observed spectral energy correlations, that yields $\xi = 0.5$ (in the case of a circumburst wind density profile) or $\xi = 0.3$ (homogeneous circumburst density). In this case, we can obtain a reasonable agreement with the data in the entire luminosity range but the very low luminosities, where the model shows a small deficit.

Table 2. Synoptic view of our findings.

Model	Fig.	Main requirement	Good fit?	Comment
Uniform, same θ_j	2	Flat below $\eta L_\star/\theta_j^2$	No	No reason. param. values
Uniform, $\theta_j(L_{iso})$	3	Needs $\theta_j \propto L_{iso}^{-\xi}$, $\xi = 0.5$ or 0.3	Yes	Marg. consistent with LL
Uniform, on/off-axis	5	Needs distrib. of θ_j and Γ	Yes	Marg. consistent with HL
Structured	7	Needs $\epsilon \propto \theta^{-4}$ or steeper	Yes	$\epsilon \propto \theta^{-2}$ excluded

(iii) In the third case the jet is still homogeneous, but it can be seen also off-axis, for viewing angles $\theta \gtrsim \theta_j$. This is possible for Γ not extreme, as illustrated in Fig. 4: the luminosity jump at $\theta_v \gtrsim \theta_j$ is more pronounced for larger Γ. The LF constructed with a single value of θ_j and Γ do not fit the data, since they show an upturn at HL instead of a steepening. On the other hand, assuming some dispersion of θ_j and Γ, we can obtain reasonable agreement. The required average values are $\langle\Gamma\rangle = 30$ and $\langle\theta_j\rangle = 3^\circ$. What is remarkable is that the analytically predicted slope at intermediate luminosities is very close to what seen.

(iv) Finally, we have investigated structured jets, of the form $\epsilon(\theta_v) \propto \theta_v^{-s}$ beyond a core angle θ_c. We have found that a good fit can be obtained, but only if the slope s is rather steep, $s > 4$, with a preferred value $s \sim 8$. This is much steeper than the value $s = 2$ originally proposed to explain the clustering of E_γ found by Frail et al. (2001).

These studies indicate that the jet must have a relatively sharp cut-off. Even if an abrupt one is unphysical (all the energy contained within θ_j, and zero outside), the energy must in any case decrease rapidly with the angle from the jet axis, once it becomes greater than the core angle θ_c. The other important overall conclusion is that although the LL bursts seem not to have enough energy to punch the progenitor star, they can nevertheless understood within the same framework of large luminosity GRBs, as long as they have a larger jet angle, or they are seen off-axis. In the first case, we see the little energy leftover after the jet break-out, in the latter case the apparent low luminosity is due to the large viewing angle, but the real energetics of these burst is much greater.

ACKNOWLEDGEMENTS

We thank the referee for constructive and positive comments. We acknowledge the 2011 PRIN-INAF grant for financial support. AP and OSS thank the Brera Observatory for the kind hospitality during their graduate work.

REFERENCES

Amati L. et al., 2002, A&A, 390, 81
Band D. L., 2002, ApJ, 578, 806
Band D. L., 2006, ApJ, 644, 378
Berger E. et al., 2003, Nature, 426, 154
Bloom J. S., Frail D. A., Kulkarni S. R., 2003, ApJ, 594, 674
Bosnjak Z., Götz D., Bouchet L., Schanne S., Cordier B., 2014, A&A, 561, A25
Bromberg O., Nakar E., Piran T., Sari R., 2012, ApJ, 749, 110
Bromberg O., Nakar E., Piran T., Sari R., 2013, ApJ, 764, 179
Butler N. R., Kocevski D., Bloom J. S., Curtis J. L., 2007, ApJ, 671, 656
Campana S. et al., 2006, Nature, 442, 1008
Campisi M. A., Li L.-X., Jakobsson P., 2010, MNRAS, 407, 1972
Cao X.-F., Yu Y.-W., Cheng K. S., Zheng X.-P., 2011, MNRAS, 416, 2174
Celotti A., Maraschi L., Ghisellini G., Caccianiga A., Maccacaro T., 1993, ApJ, 416, 118
Chapman R., Tanvir N. R., Priddey R. S., Levan A. J., 2007, MNRAS, 382, L21
Cui X., Liang E., Lu R., 2005, AJ, 130, 418
Daigne F., Mochkovitch R., 2007, A&A, 465, 1
Daigne F., Rossi E. M., Mochkovitch R., 2006, MNRAS, 372, 1034
Firmani C., Avila-Reese V., Ghisellini G., Tutukov A. V., 2004, ApJ, 611, 1033
Firmani C., Ghisellini G., Ghirlanda G., Avila-Reese V., 2005, MNRAS, 360, L1
Frail D. A. et al., 2000, ApJ, 538, L129
Frail D. A. et al., 2001, ApJ, 562, L55
Frail D. A., Soderberg A. M., Kulkarni S. R., Berger E., Yost S., Fox D. W., Harrison F. A., 2005, ApJ, 619, 994
Galama T. J., Vreeswijk P. M., van Paradijs J., 1998, Nature, 395, 670
Ghirlanda G., Ghisellini G., Lazzati D., 2004, ApJ, 616, 331
Ghirlanda G., Ghisellini G., Firmani C., 2005, MNRAS, 361, L10
Ghirlanda G., Nava L., Ghisellini G., Firmani C., 2007, A&A, 466, 127
Ghirlanda G. et al., 2013, MNRAS, 428, 1410
Ghisellini G., Ghirlanda G., Mereghetti S., Bosnjak Z., Tavecchio F., Firmani C., 2006, MNRAS, 372, 1699
Ghisellini G., Celotti A., Ghirlanda G., Firmani C., Nava L., 2007, MNRAS, 382, L72
Ghisellini G., Lazzati D., 1999, MNRAS, 309, L7
Guetta D., Granot J., Begelman M. C., 2005, ApJ, 622, 482
Howell E. J., Coward D. M., Stratta G., Gendre B., Zhou H., 2014, MNRAS, 444, 28
Jakobsson P. et al., 2012, ApJ, 752, 62
Jimenez R., Band D., Piran T., 2001, ApJ, 561, 171
Kumar P., Smoot G. F., 2014, MNRAS, 445, 528
Lazzati D., Begelman M. C., 2005, ApJ, 629, 903
Lazzati D., Rossi E., Ghisellini G., Rees M. J., 2004, MNRAS, 347, L1
Leloudas G., Fynbo J. P. U., Schulze S., Xu D., Malesani D., Geier S., Cano Z., Jakobsson P., 2013, GRB Coordinates Network, 14983, 1
Levinson A., Eichler D., 2003, ApJ, 594, L19
Liang E., Zhang B., Virgili F., Dai Z. G., 2007, ApJ, 662, 1111
Lipunov V. M., Postnov K. A., Prokhorov M. E., 2001, Astron. Rep., 45, 236
Lloyd-Ronning N. M., Dai X., Zhang B., 2004, ApJ, 601, 371
Lyutikov M., Blandford R., 2002, in Ouyed R., Conf. on Beaming and Jets in Gamma Ray Bursts. Available at: http://www.slac.stanford.edu/econf/0208122
Morsony B. J., Lazzati D., Begelman M. C., 2010, ApJ, 723, 267
Mészáros P., Rees M. J., 2001, ApJ, 556, L37
Nakar E., Granot J., Guetta D., 2004, ApJ, 606, L37
Natarajan P., Albanna B., Hjorth J., Ramirez-Ruiz E., Tanvir N., Wijers R., 2005, MNRAS, 364, L8
Nava L., Ghisellini G., Ghirlanda G., Tavecchio F., Firmani C., 2006. A&A, 450, 471
Panaitescu A., Kumar P., 2002, ApJ, 571, 779
Peng F., Königl A., Granot J., 2005, ApJ, 626, 966
Perna R., Sari R., Frail D., 2003, ApJ, 594, 379
Perley D. A., Foley R. J., Bloom J. S., Butler N. R., 2006, GRB Coordinates Network, 5387, 1
Pian E. et al., 2006, Nature, 442, 1011
Prochaska J. X., Bloom J. S., Chen H. W., Hurley K., Dressler A., Osip D., 2003, GRB Circular Network, 2482, 1

Ramirez-Ruiz E., Celotti A., Rees M. J., 2002, MNRAS, 337, 1349
Rees M. J., Meszaros P., 1994, ApJ, 430, L93
Rhoads J. E., 1997, ApJ, 487, L1
Rossi E., Lazzati D., Rees M. J., 2002, MNRAS, 332, 945
Rossi E. M., Davide L., Jay D. S., Gabriele G., 2004, MNRAS, 354, 86
Sakamoto T. et al., 2004, ApJ, 602, 875
Sakamoto T. et al., 2009, ApJ, 693, 922
Salvaterra R., Chincarini G., 2007, ApJ, 656, L49
Salvaterra R., Guidorzi C., Campana S., Chincarini G., Tagliaferri G., 2009, MNRAS, 396, 299
Salvaterra R. et al., 2012, ApJ, 749, 68 (S12)
Sari R., Piran T., Halpern J. P., 1999, ApJ, 519, L17
Sazonov S. Yu., Lutovinov A. A., Sunyaev R. A., 2004, Nature, 430, 646
Shahmoradi A., 2013, ApJ, 766, 111
Sheth K., Frail D. A., White S., Das M., Bertoldi F., Walter F., Kulkarni S. R., Berger E., 2003, ApJ, 595, L33
Shivvers I., Berger E., 2011, ApJ, 734, 58
Soderberg A. M. et al., 2002, GRB Coordinates Network, 1554, 1
Soderberg A. M. et al., 2006, Nature, 442, 1014
Sollerman J. et al., 2006, A&A, 454, 503
Starling R. L. C., Wijers R. A. M. J., Hughes M. A., Tanvir N. R., Vreeswijk P. M., Rol E., Salamanca I., 2005, MNRAS, 360, 305
Tan J. C., Matzner C. D., McKee C. F., 2001, ApJ, 551, 946
Tanvir N. R., Levan A. J., Cucchiara A., Fox D. B., 2012, GRB Coordinates Network, 13251, 1
Thoene C. C., Fynbo J. P. U., Sollerman J., Jensen B. L., Hjorth J., Jakobsson P., Klose S., 2006, GRB Coordinates Network, 5161, 1
Troja E., Cusumano G., Laparola V., Mangano V., Mineo T., 2006, Il Nuovo Cimento B, 121, 1599
Ulanov M. V., Golenetskii S. V., Frederiks D. D., Mazets R. L., Aptekar E. P., Kokomov A. A., Palshin V. D., 2005, Il Nuovo Cimento C, 28, 351
Urry C. M., Shafer R. A., 1984, ApJ, 280, 569
van Eerten H. J., MacFadyen A. I., 2012, ApJ, 751, 155
Virgili F. J., Liang E.-W., Zhang B., 2009, MNRAS, 392, 91
Vlahakis N., Peng F., Königl A., 2003, ApJ, 594, L23
von Kienlin A. et al., 2014, ApJS, 211, 13
Wanderman D., Piran T., 2010, MNRAS, 406, 1944 (WP10)
Wanderman D., Piran T., 2014, MNRAS, preprint (arXiv:1405.5878)
Yonetoku D., Murakami T., Nakamura T., Yamazaki R., Inoue A. K., Ioka K., 2004, ApJ, 609, 935
Zhang B., Meszaros P., 2002, ApJ, 571, 876
Zhang W., Woosley S. E., MacFadyen A. I., 2003, ApJ, 586, 356
Zhang W., Woosley S. E., Heger A., 2004, ApJ, 608, 365
Zhang B.-B. et al., 2012, ApJ, 756, 190

This paper has been typeset from a TEX/LATEX file prepared by the author.